Late-time interacting cosmologies and the Hubble constant tension

Stefano Gariazzo[1,*], Eleonora Di Valentino,[2,†] Olga Mena,[3,‡] and Rafael C. Nunes[4,5,§]

[1]*Istituto Nazionale di Fisica Nucleare (INFN), Sezione di Torino, Via P. Giuria 1, I-10125 Turin, Italy*
[2]*School of Mathematics and Statistics, University of Sheffield,*
Hounsfield Road, Sheffield S3 7RH, United Kingdom
[3]*IFIC, Universidad de Valencia-CSIC, 46071 Valencia, Spain*
[4]*Instituto de Física, Universidade Federal do Rio Grande do Sul, 91501-970 Porto Alegre RS, Brazil*
[5]*Divisão de Astrofísica, Instituto Nacional de Pesquisas Espaciais, Avenida dos Astronautas 1758,*
São José dos Campos, 12227-010 São Paulo, Brazil

In this manuscript we reassess the potential of interacting dark matter–dark energy models in solving the Hubble constant tension. These models have been proposed but also questioned as possible solutions to the H_0 problem. Here we examine several interacting scenarios against cosmological observations, focusing on the important role played by the calibration of supernovae data. In order to reassess the ability of interacting dark matter–dark energy scenarios in easing the Hubble constant tension, we systematically confront their theoretical predictions using a prior on the supernovae Ia absolute magnitude M_B, which has been argued to be more robust and certainly less controversial than using a prior on the Hubble constant H_0. While some data combinations do not show any preference for interacting dark sectors and in some of these scenarios the clustering σ_8 tension worsens, interacting cosmologies with a dark energy equation of state $w < -1$ are preferred over the canonical ΛCDM picture even with cosmic microwave background data alone and also provide values of σ_8 in perfect agreement with those from weak lensing surveys. Future cosmological surveys will test these exotic dark energy cosmologies by accurately measuring the dark energy equation of state and its putative redshift evolution.

I. INTRODUCTION

A plethora of observations have led to confirm the standard ΛCDM framework as the most economical and successful model describing our current Universe. This simple picture (pressureless dark matter, baryons and a cosmological constant representing the vacuum energy) has been shown to provide an excellent fit to cosmological data. However, there are a number of inconsistencies that persist and, instead of diluting with improved precision measurements, gain significance [1–11].

The most exciting (i.e., probably not due to systematics) and most statistically significant (4–6σ) tension [12–14] in the literature is the so-called Hubble constant tension, which refers to the discrepancy between cosmological predictions and low-redshift estimates of H_0. Within the ΛCDM scenario, cosmic microwave background (CMB) measurements from the *Planck* satellite provide a value of $H_0 = 67.36 \pm 0.54 \text{ km s}^{-1} \text{ Mpc}^{-1}$ at 68% C.L. [15]. Near-Universe, local measurements of H_0, using the cosmic distance ladder calibration of type Ia supernovae with Cepheids, as those carried out by the SH0ES team, provide a measurement of the Hubble constant $H_0 = 73.04 \pm 1.04 \text{ km s}^{-1} \text{ Mpc}^{-1}$ at 68% C.L. [16]. This problematic $\sim 5\sigma$ discrepancy aggravates when considering other late-time estimates of H_0. For instance, measurements from the megamaser cosmology project [17] or those exploiting surface brightness fluctuations [18] or type II supernovae [19] only exacerbate this tension. Nevertheless, there are measurements from other probes that are still unable to disentangle between the nearby Universe and CMB measurements. These include results from the tip of the Red Giant Branch (TRGB) [5], from the astrophysical strong lensing observations [20] or from gravitational wave events [21]. It is important to mention that the differences in H_0 measurements between the SHOES and the TRGB approaches arise because the TRGB sample and the Cepheids are modeled as different distance indicators, in many cases belonging to the same host galaxies; see Ref. [16] for an updated discussion. Thus, in principle, this difference may not arise from a different treatment of SNe Ia sample. On the other hand, several CMB-free analyses (in general, model-dependent analysis) were performed to constraint H_0 (see Refs. [22–29] for a short

[*]gariazzo@to.infn.it
[†]e.divalentino@sheffield.ac.uk
[‡]omena@ific.uv.es
[§]rafadcnunes@gmail.com

list). Therefore, there is a crucial lack of consensus in the current extraction of the Hubble constant. The main goal of this manuscript is to scrutinize the ability of some possible late-time nonstandard cosmologies to solve the issue.

As previously mentioned, the SH0ES Collaboration exploits the cosmic distance ladder calibration of type Ia supernovae, which means that these observations do not provide a direct extraction of the Hubble parameter. More concretely, the SH0ES team [30] measures the absolute peak magnitude M_B of type Ia supernovae *standard candles* and then translates these measurements into an estimate of H_0 by means of the magnitude-redshift relation of the Pantheon type Ia supernovae sample [31]. Therefore, strictly speaking, the SH0ES team does not directly extract the value of H_0, and there have been arguments in the literature aiming to translate the Hubble constant tension into a type Ia supernovae absolute magnitude tension M_B [32–34].

A number of studies have prescribed to use in the statistical analyses a prior on the intrinsic magnitude rather than on the Hubble constant H_0 [7,34–37]. A prior on M_B is more robust and avoids double-counting issues when using simultaneously luminosity distance measurements from the SN Ia Pantheon sample and measurements of H_0 from SH0ES. In this regard, the value of H_0 may also be affected by the choice of the expansion history fit; see Ref. [33]. We address here in the following the potential of interacting dark matter–dark energy cosmology [38] in resolving the Hubble constant tension (see Refs. [14,39–69], and references therein) by demonstrating explicitly from a full analysis that the performance of the model still holds when applying a prior on M_B (see also the recent Ref. [70]).

II. THEORETICAL FRAMEWORK

We adopt a flat cosmological model described by the Friedmann-Lemaître-Robertson-Walker metric. A possible parametrization of a dark matter–dark energy interaction is provided by the following expressions [71,72]:

$$\nabla_\mu T^\mu_{(dm)\nu} = Q u^{(dm)}_\nu / a, \qquad (1)$$

$$\nabla_\mu T^\mu_{(de)\nu} = -Q u^{(dm)}_\nu / a. \qquad (2)$$

In the equations above, $T^\mu_{(dm)\nu}$ and $T^\mu_{(de)\nu}$ represent the energy-momentum tensors for the dark matter and dark energy components, respectively, the function Q is the interaction rate between the two dark components, and $u^{(dm)}_\nu$ represents the dark matter four-velocity. In what follows we shall restrict ourselves to the case in which the interaction rate is proportional to the dark energy density ρ_{de} [71,72]:

$$Q = \delta_{\mathrm{DMDE}} \mathcal{H} \rho_{de}, \qquad (3)$$

where δ_{DMDE} is a dimensionless coupling parameter and $\mathcal{H} = \dot{a}/a$.[1] The background evolution equations in the coupled model considered here read [73]

$$\dot{\rho}_{dm} + 3\mathcal{H}\rho_{dm} = \delta_{\mathrm{DMDE}}\mathcal{H}\rho_{de}, \qquad (4)$$

$$\dot{\rho}_{de} + 3\mathcal{H}(1 + w_{0,\mathrm{fld}})\rho_{de} = -\delta_{\mathrm{DMDE}}\mathcal{H}\rho_{de}. \qquad (5)$$

The evolution of the dark matter and dark energy density perturbations and velocities divergence field are described in Ref. [50] and references therein. We use this modeling to describe the linear perturbation dynamics evolution of the model under consideration in this work. Some of the main effects on the formation of structures in large scales were recently reviewed in detail in Ref. [74].

It has been shown in the literature that this model is free of instabilities if the sign of the coupling δ_{DMDE} and the sign of $(1 + w_{0,\mathrm{fld}})$ are opposite, where $w_{0,\mathrm{fld}}$ refers to the dark energy equation of state [72,75]. In order to satisfy such stability conditions, we explore three possible scenarios, all of them with a redshift-independent equation of state. In model A, the equation of state $w_{0,\mathrm{fld}}$ is fixed to -0.999. Consequently, since $(1 + w_{0,\mathrm{fld}}) > 0$, in order to ensure an instability-free perturbation evolution, the dark matter–dark energy coupling δ_{DMDE} is allowed to vary in a negative range. In model B, $w_{0,\mathrm{fld}}$ is allowed to vary but we ensure that the condition $(1 + w_{0,\mathrm{fld}}) > 0$ is always satisfied. Therefore, the coupling parameter δ_{DMDE} is negative. In model C, instead, the dark energy equation of state is phantom ($w_{0,\mathrm{fld}} < -1$); therefore, the dark matter–dark energy coupling is taken as positive to avoid early-time instabilities.

The coupling function Q can take different forms. For instance, it may be proportional to ρ_{dm} [76–78] or $\rho_{de} + \rho_{dm}$ [78,79], as well as other phenomenological forms [80,81], or admit a general covariant framework [82,83]. Admitting a general interaction coupling function and under reasonable physical stability conditions, it is possible to restrict the function Q in several ways [83]. In addition, the authors in Ref. [84], show interaction rates featuring factors proportional to H, including but not limited to the case considered here, may naturally emerge when considering well-motivated and simple field theories for the coupling in the dark sector.

As discussed above, we shall present separately the cosmological constraints for three models based on the parametrization Eq. (3), together with those corresponding to the canonical ΛCDM case.

---

[1]The dot indicates derivative with respect to conformal time $d\tau = dt/a$.

III. DATASETS AND METHODOLOGY

In this section, we present the datasets and methodology employed to obtain the observational constraints on the model parameters by performing Bayesian Monte Carlo Markov chain analyses. In order to constrain the parameters, we use the following datasets.

(i) *The CMB temperature and polarization power spectra from the final release of Planck 2018.*—In particular, we adopt the plikTTTEEE + lowl + lowE likelihood [85,86], plus the CMB lensing reconstruction from the four-point correlation function [87].

(ii) *Type Ia supernovae (SN) distance moduli measurements from the Pantheon sample [31].*—These measurements constrain the uncalibrated luminosity distance $H_0 d_L(z)$ or in other words the slope of the late-time expansion rate (which in turn constrains the current matter energy density $\Omega_{0,\mathrm{m}}$), where d_L is given by

$$d_L(z) = c(1+z) \int \frac{dz}{H(z)}. \qquad (6)$$

(iii) *Baryon acoustic oscillation (BAO) distance and expansion rate measurements from the 6dFGS [88], SDSS-DR7 MGS [89], and BOSS DR12 [90] galaxy surveys, as well as from the eBOSS DR14 Lyman-α (Lyα) absorption [91] and Lyα-quasar cross-correlation [92].*—These consist of isotropic BAO measurements of $D_V(z)/r_d$ [with $D_V(z)$ and r_d the spherically averaged volume distance and sound horizon at baryon drag, respectively] for 6dFGS and MGS and anisotropic BAO measurements of $D_M(z)/r_d$ and $D_H(z)/r_d$ [with $D_M(z)$ the comoving angular diameter distance and $D_H(z) = c/H(z)$ the radial distance] for BOSS DR12, eBOSS DR14 Lyα, and eBOSS DR14 Lyα-quasar cross-correlation.

(iv) *A Gaussian prior on $M_B = -19.244 \pm 0.037$ mag [34], corresponding to the SN measurements from SH0ES [30].*—When used, this prior is considered over all the Pantheon sample.

For the sake of brevity, data combinations are indicated as CMB (C), CMB+BAO (CB), CMB+SN (CS), CMB+SN+BAO (CSB) and CMB + SN + BAO + M_B (CSBM).

Cosmological observables are computed with CLASS [93,94]. In order to derive bounds on the proposed scenarios, we modify the efficient and well-known cosmological package MontePython [95], supporting the Planck 2018 likelihood [96]. We make use of CalPriorSNIa, a module for MontePython [97], that implements an effective calibration prior on the absolute magnitude of type Ia supernovae [34,98].

IV. MAIN RESULTS AND DISCUSSION

We start by discussing the results obtained within the canonical ΛCDM scenario. Table II presents the mean values and the 1σ errors on a number of different cosmological parameters within this standard scenario. Namely, we show the constraints on $\omega_{\mathrm{cdm}} \equiv \Omega_{0,\mathrm{cdm}}h^2$, the current dark energy density $\Omega_{0,\mathrm{fld}}$, the supernovae Ia intrinsic magnitude M_B, the Hubble constant H_0 and the clustering parameter σ_8 arising from the data combinations considered here and above described: CMB (C), CMB + BAO (CB), CMB + SN (CS), CMB + SN + BAO (CSB) and CMB + SN + BAO + M_B (CSBM).

Interestingly, *none* of the parameters barely change their mean values when combining CMB data with additional datasets, except for the case when we consider the prior on the supernova Ia absolute magnitude M_B. In this particular case, the value of H_0 is mildly larger (and, consequently, the values of ω_{cdm} and σ_8 mildly smaller); see the black curves depicted in Fig. 1 for the CSBM data combination. Nevertheless, the parameter ranges agree within 1σ and therefore within the ΛCDM picture. This statement can be

TABLE I. Priors of $w_{0,\mathrm{fld}}$, δ in models A, B, and C.

Model	Prior $w_{0,\mathrm{fld}}$	Prior δ_{DMDE}
A	−0.999	[−1.0, 0.0]
B	[−0.999, −0.333]	[−1.0, 0.0]
C	[−3, −1.001]	[0.0, 1.0]

TABLE II. Mean values and 68% C.L. errors on $\omega_{\mathrm{cdm}} \equiv \Omega_{\mathrm{cdm}}h^2$, the current dark energy density $\Omega_{0,\mathrm{fld}}$, the supernovae Ia intrinsic magnitude M_B, the Hubble constant H_0 and the clustering parameter σ_8 within the standard ΛCDM paradigm. We also report the minimum value of the χ^2 function obtained for each of the data combinations.

| Parameter	C	CB	CS	CSB	CSBM
ω_{cdm}	0.1200 ± 0.0012	$0.11948^{+0.00092}_{-0.00090}$	0.1198 ± 0.0011	$0.11930^{+0.00089}_{-0.00091}$	0.11831 ± 0.00090
$\Omega_{0,\mathrm{fld}}$	$0.6850^{+0.0074}_{-0.0077}$	$0.6882^{+0.0054}_{-0.0056}$	$0.6864^{+0.0069}_{-0.0070}$	0.6893 ± 0.0054	0.6957 ± 0.0053
M_B	$\cdots$	$\cdots$	-19.422 ± 0.014	-19.416 ± 0.011	-19.401 ± 0.011
H_0	$67.38^{+0.56}_{-0.55}$	$67.62^{+0.42}_{-0.41}$	67.50 ± 0.51	67.71 ± 0.40	$68.20^{+0.41}_{-0.40}$
σ_8	$0.8114^{+0.0057}_{-0.0059}$	$0.8106^{+0.0058}_{-0.0056}$	$0.8113^{+0.0063}_{-0.0061}$	$0.8107^{+0.0060}_{-0.0057}$	$0.8090^{+0.0060}_{-0.0063}$
Minimum χ^2	2780.70	2792.82	3808.42	3820.76	3840.58
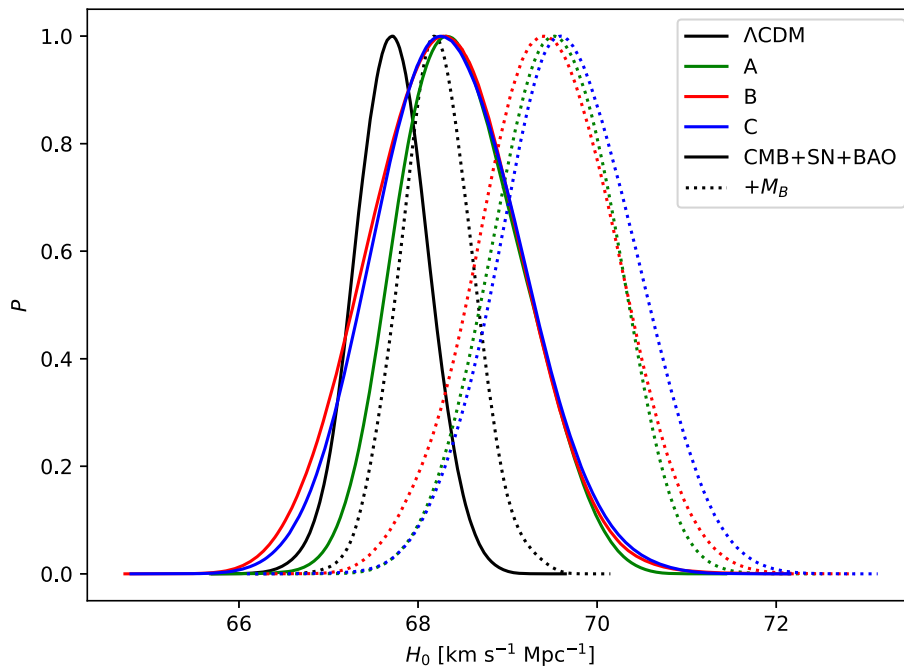
FIG. 1.   Posterior distribution of the Hubble parameter in the ΛCDM model (black) and in interacting cosmologies, with priors on the parameters as given in Table I. We show constraint obtained within model A (green), model B (red) and model C (blue) for the CMB + SN + BAO data combination (solid lines) and CMB + SN + BAO + M_B (dotted lines).

clearly confirmed from the contours illustrated in Fig. 2, which presents the two-dimensional allowed contours and the one-dimensional posterior probabilities on the parameters shown in Table II. This is because the CSB combination is the leading ingredient in the likelihood, and therefore all the parameters, including M_B and H_0, are barely modified with respect to their values within the CSB case, when considering the M_B prior. Nevertheless, there is an increase in the value of the minimum χ^2 of $\sim$20 when adding the prior on the SN absolute magnitude.

We focus now on model A, which refers to an interacting cosmology with $w_{0,\text{fld}} = -0.999$ and $\delta_{\text{DMDE}} < 0$. Table III presents the mean values and the 1σ errors on the same cosmological parameters listed above, with the addition of the coupling parameter δ_{DMDE}, for the very same data combination already discussed. Notice that the minimum values of the χ^2 are always smaller than those found for the minimal ΛCDM scheme for the very same data combinations: therefore, the addition of a coupling *improves* (mildly, in some cases) the overall fit. Indeed, the $\Delta\chi^2$ between the CSBM and CSB datasets is now $\sim$16, i.e., less than within the ΛCDM case. We also quantify here how much the fit improves by considering an information criteria that has been widely exploited in astrophysical and cosmological contexts, namely the frequentist Akaike information criterion (AIC) [99,100], which establishes that the penalty term between competing models is twice the number of free parameters in the model and consequently penalizes more complex models that give similar χ^2

values. The best model is the one minimizing the AIC test: in our tables, positive values prefer ΛCDM scenarios, while negative ones favor the interacting models. The significance against a given model will be judged based on the Jeffreys' scale, which will characterize a difference Δ AIC > 5 (> 10) as a strong (decisive) evidence against the cosmological model with a higher value for the AIC test. Notice from Table III that data combinations C, CB, CS and CSB show a very mild, almost negligible preference for the ΛCDM model, while the CSBM data combination prefers a model with a dark sector coupling, leading to the largest Δ_{AIC} (in absolute value). This implies that the addition of a dark sector interaction slightly alleviates the tension within the standard ΛCDM paradigm concerning the inferred values of the supernova Ia absolute magnitude M_B and that this statement still holds when applying a prior on M_B and not on H_0, as the former is considered to be more robust than the latter. The value of the Hubble constant within the interacting scenario A is larger (regardless of the dataset combination) than the one obtained in the ΛCDM framework (see Fig. 1), especially for the CMB data alone case: due to the extra contribution from the dark energy component, the amount of intrinsic dark matter should be small and therefore, to leave unchanged the CMB temperature anisotropy peak structure, the value of H_0 must be larger. In addition, one can notice that the value of $\Omega_{0,\text{fld}}$ is much larger. The reason for this is again related to the lower value for the present matter energy density $\Omega_{0,\text{m}}$, which is required within the interacting cosmologies when
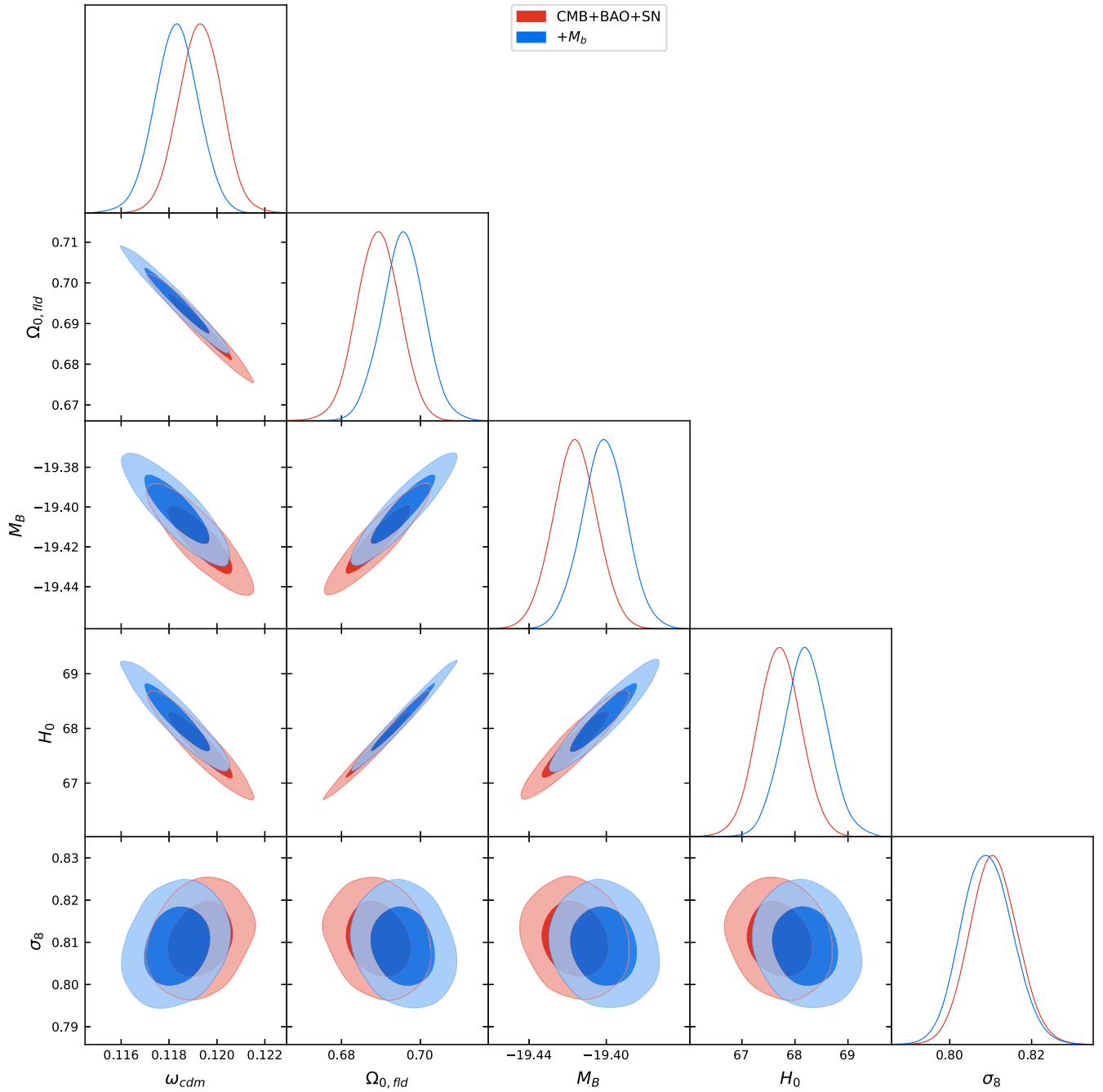
FIG. 2. 68% C.L. and 95% C.L. allowed contours and one-dimensional posterior probabilities on a selection of cosmological parameters within the canonical ΛCDM picture, considering two data combinations: CMB + SN + BAO (red) and CMB + SN + BAO + M_B (blue).

the dark matter–dark energy coupling is negative. In the context of a universe with a negative dark coupling, indeed, there is an energy flow from dark matter to dark energy. Consequently, the (dark) matter content in the past is higher than in the standard ΛCDM scenario and the amount of intrinsic (dark) matter needed today is lower because of the extra contribution from the dark energy sector. In a flat universe, this translates into a much higher value of $\Omega_{0,\text{fld}}$.

The mean values of the parameters in the CSBM data combination (in which the preferred model is the interacting one) are, in general, in a decent agreement with the mean values obtained within other dataset combinations; see Table III. Interestingly, we observe a $> 2\sigma$ indication in favor of a nonzero value of the coupling δ_{DMDE} when considering the CSBM data combinations. Figure 3 presents the two-dimensional allowed contours and the

TABLE III. Mean values and 68% C.L. errors or 95% C.L. limits on $\omega_{cdm} \equiv \Omega_{cdm}h^2$, the current dark energy density $\Omega_{0,fld}$, the dimensionless dark matter–dark energy coupling δ_{DMDE}, the supernovae Ia intrinsic magnitude M_B, the Hubble constant H_0 and the clustering parameter σ_8 within the interacting model A; see Table I. We also report the minimum value of the χ^2 function obtained for each of the data combinations and the AIC test with respect to the ΛCDM case.

Parameter	C	CB	CS	CSB	CSBM
ω_{cdm}	$0.075^{+0.040}_{-0.027}$	$0.1062^{+0.0124}_{-0.0083}$	$0.1082^{+0.0091}_{-0.0067}$	$0.1094^{+0.0084}_{-0.0062}$	$0.0986^{+0.0091}_{-0.0090}$
$\Omega_{0,fld}$	$0.806^{+0.072}_{-0.092}$	$0.726^{+0.025}_{-0.034}$	$0.720^{+0.020}_{-0.026}$	$0.717^{+0.019}_{-0.023}$	$0.748^{+0.023}_{-0.024}$
δ_{DMDE}	> -0.75	> -0.36	$-0.109^{+0.104}_{-0.043}$	> -0.24	$-0.182^{+0.080}_{-0.077}$
M_B	$\cdots$	$\cdots$	$-19.402^{+0.019}_{-0.020}$	$-19.402^{+0.015}_{-0.016}$	$-19.377^{+0.015}_{-0.014}$
H_0	$71.18^{+2.31}_{-2.97}$	$68.70^{+0.86}_{-1.03}$	$68.46^{+0.78}_{-0.86}$	$68.45^{+0.64}_{-0.72}$	$69.51^{+0.70}_{-0.65}$
σ_8	$1.21^{+0.36}_{-0.43}$	$0.907^{+0.064}_{-0.096}$	$0.893^{+0.048}_{-0.071}$	$0.881^{+0.045}_{-0.064}$	$0.963^{+0.077}_{-0.085}$
Minimum χ^2	2779.16	2792.78	3807.54	3819.12	3836.00
Δ_{AIC}	0.46	1.96	1.12	0.36	-2.58

one-dimensional posterior probabilities obtained within model A. Even if within this interacting scenario there is an $\sim 2\sigma$ indication for a nonzero dark matter–dark energy coupling when considering either H_0 or M_B measurements, the value of the Hubble constant is mildly larger than within the standard ΛCDM model, and the model is preferred over the former one applying the AIC criterion to the CSBM data combination (which includes the prior on the SN Ia absolute magnitude M_B), the values of the clustering parameter σ_8 are larger than those within the minimal ΛCDM picture, increasing the tension with weak lensing surveys. For instance, the latest results from the Dark Energy Survey [101] (see also results for the KiDS-1000 photometric survey [102]) provide $\sigma_8 = 0.733^{+0.039}_{-0.049}$ (assuming a ΛCDM model) and therefore the addition of a coupling increases the well-known tension between measurements of σ_8 at high and low redshifts.

Focusing now on model B (see Table IV), which assumes a negative coupling δ_{DMDE} and a constant, but freely varying, dark energy equation of state $w_{0,fld}$ within the $w_{0,fld} > -1$ region, we notice, as in model A, a smaller value of the matter density and a larger value of the Hubble parameter (see Fig. 1) to compensate for the effect of the energy flow between the dark energy and dark matter sectors. The value of H_0, however, is slightly smaller than in model A, due to the strong anticorrelation between $w_{0,fld}$ and H_0 [50,103], since a larger value of $w_{0,fld} > -1$ implies a lower value of H_0. Nevertheless, a mild preference (up to $\sim 2\sigma$) for a nonzero value of the dark matter–dark energy coupling is present also in this case, for four out of the five data combinations presented in this study.

Notice that the minimum χ^2 in model B is smaller than that corresponding to the minimal ΛCDM framework and also smaller than that of model A, which is nested in model B, as expected. However there is no indication for a

preference of this model B over the ΛCDM canonical one from the C, CB, CS and CSB datasets, as can be inferred from the values of Δ_{AIC} shown in Table IV. Moreover, even if $\Delta_{AIC} < 0$ for the CSBM case, its value is very small and therefore not statistically significant.

In Fig. 4 we depict the two-dimensional allowed contours and the one-dimensional posterior probabilities obtained for model B. From a comparison to Fig. 2 and also confronting the mean values of Table IV to those shown in Table II (and, to a minor extent, to those in Table III), one can notice that the value of $\Omega_{0,fld}$ is again much larger, due to the lower value of $\Omega_{m,0}$. On the other hand, a lower value of $\Omega_{m,0}$ requires a larger value of the clustering parameter σ_8 to be able to satisfy the overall normalization of the matter power spectrum, exacerbating the σ_8 tension with DES [101] and KiDS-1000 [102] results.

Finally, Table V shows the mean values and the 1σ errors on the usual cosmological parameters explored along this study, for model C. Notice that this model benefits both from its interacting nature and from the fact that $w_{0,fld} < -1$ and $\delta_{DMDE} > 0$. Both features of the dark energy sector have been shown to be excellent solutions to the Hubble constant problem. Indeed, within this model, the value of the Hubble constant is naturally larger than within the ΛCDM model (see the blue lines in Fig. 1), regardless of the datasets assumed in the analyses. Despite its phantom nature, as in this particular case $w_{0,fld} < -1$ to ensure a instability-free evolution of perturbations, model C provides the *best fits to any of the data combinations explored here, performing even better than* the minimal ΛCDM picture, as one can clearly notice from the results of Table V. In addition, the AIC criterion shows that not only the CSBM data combination, but also CMB data alone do prefer this model over the minimal ΛCDM picture.
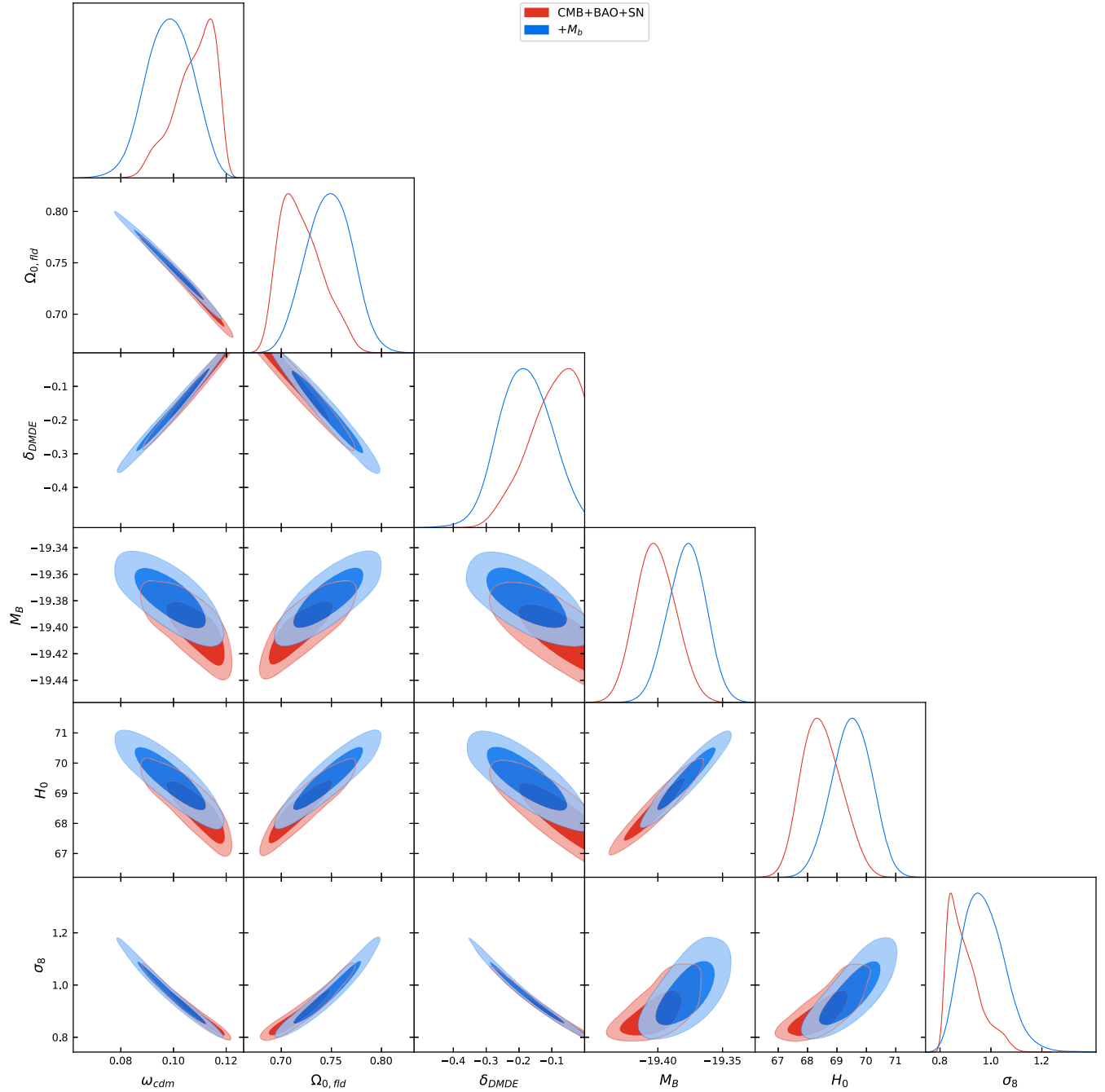
FIG. 3. 68% C.L. and 95% C.L. allowed contours and one-dimensional posterior probabilities on a selection of cosmological parameters within model A, considering two data combinations: CMB + SN + BAO (black) and CMB + SN + BAO + M_B (blue).

TABLE IV. Mean values and 68% C.L. errors or 95% C.L. limits on $\omega_{cdm} \equiv \Omega_{cdm} h^2$, the current dark energy density $\Omega_{0,fld}$, the dark energy equation of state $w_{0,fld}$, the dimensionless dark matter–dark energy coupling δ_{DMDE}, the supernovae Ia intrinsic magnitude M_B, the Hubble constant H_0 and the clustering parameter σ_8 within the interacting model B; see Table I. We also report the minimum value of the χ^2 function obtained for each of the data combinations and the AIC test with respect to the ΛCDM case.

Parameter	C	CB	CS	CSB	CSBM
ω_{cdm}	$0.069^{+0.040}_{-0.039}$	$0.085^{+0.028}_{-0.020}$	$0.087^{+0.024}_{-0.020}$	$0.087^{+0.024}_{-0.019}$	$0.074^{+0.028}_{-0.023}$
$\Omega_{0,fld}$	0.81 ± 0.11	$0.768^{+0.053}_{-0.063}$	$0.764^{+0.048}_{-0.056}$	$0.765^{+0.044}_{-0.055}$	$0.800^{+0.051}_{-0.061}$

(Table continued)

TABLE IV. *(Continued)*

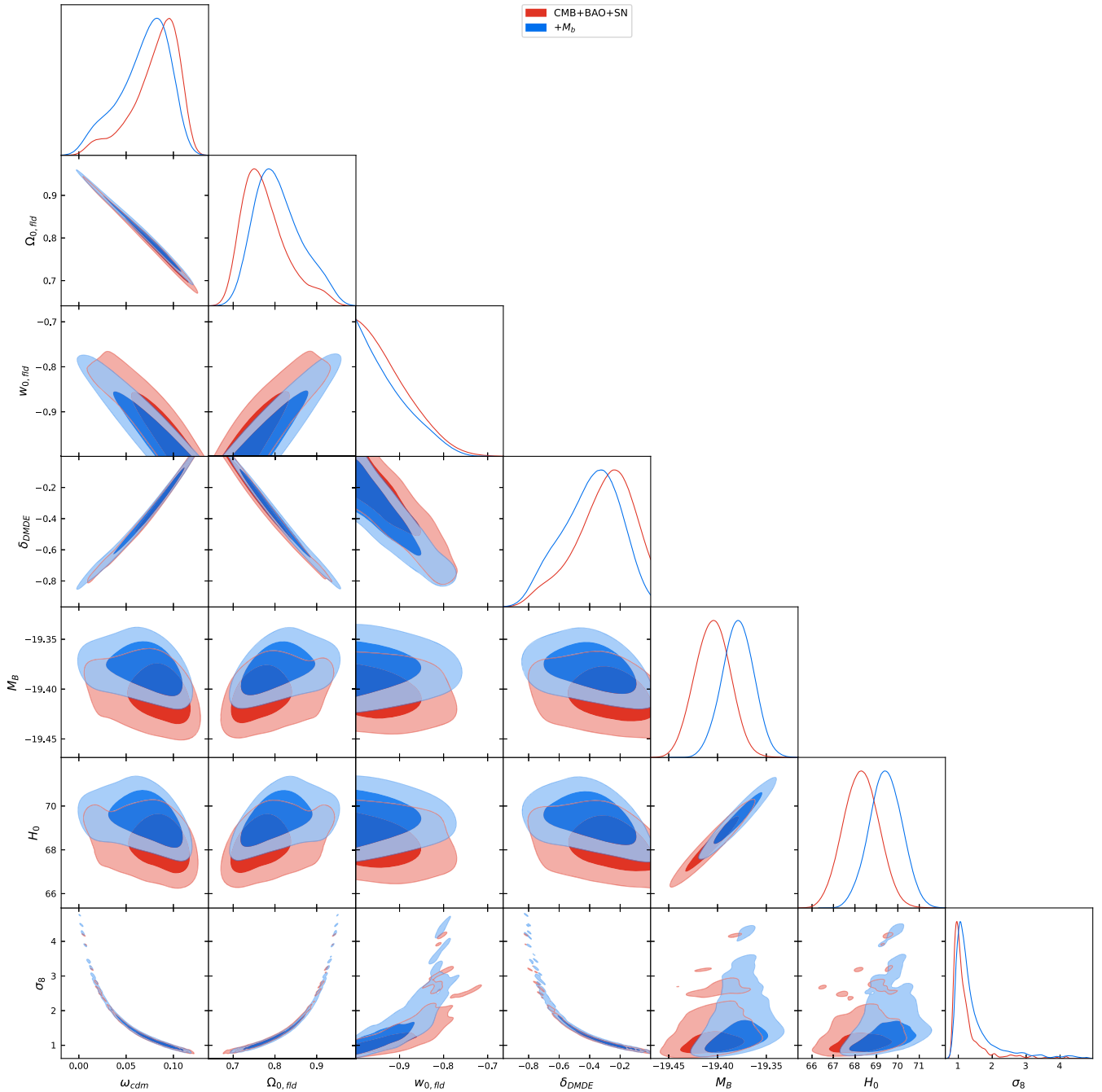| Parameter	C	CB	CS	CSB	CSBM
$w_{0,\text{fld}}$	< -0.73	< -0.80	< -0.82	< -0.81	< -0.81
δ_{DMDE}	> -0.78	$-0.30^{+0.27}_{-0.12}$	$-0.29^{+0.20}_{-0.16}$	$-0.28^{+0.21}_{-0.15}$	$-0.38^{+0.21}_{-0.18}$
M_B	$\cdots$	$\cdots$	$-19.407^{+0.023}_{-0.022}$	$-19.405^{+0.017}_{-0.018}$	-19.379 ± 0.016
H_0	$68.72^{+3.50}_{-3.40}$	$68.26^{+1.18}_{-1.24}$	$68.21^{+1.02}_{-1.00}$	$68.28^{+0.83}_{-0.82}$	$69.42^{+0.79}_{-0.71}$
σ_8	$1.27^{+0.51}_{-0.54}$	$1.07^{+0.18}_{-0.27}$	$1.06^{+0.19}_{-0.23}$	$1.06^{+0.17}_{-0.22}$	$1.21^{+0.27}_{-0.34}$
Minimum χ^2	2778.16	2792.42	3807.22	3818.96	3836.02
Δ_{AIC}	1.46	3.60	2.80	2.20	-0.56

FIG. 4. 68% C.L. and 95% C.L. allowed contours and one-dimensional posterior probabilities on a selection of cosmological parameters within model B, considering two data combinations: CMB + SN + BAO (red) and CMB + SN + BAO + M_B (blue).

TABLE V. Mean values and 68% C.L. errors or 95% C.L. limits on $\omega_{cdm} \equiv \Omega_{cdm} h^2$, the current dark energy density $\Omega_{0,fld}$, the current matter energy density $\Omega_{0,m}$, the dark energy equation of state $w_{0,fld}$, the dimensionless dark matter–dark energy coupling δ_{DMDE}, the supernovae Ia intrinsic magnitude M_B, the Hubble constant H_0 and the clustering parameter σ_8 within the interacting model C; see Table I. We also report the minimum value of the χ^2 function obtained for each of the data combinations and the AIC test with respect to the ΛCDM case.

Parameter	C	CB	CS	CSB	CSBM
ω_{cdm}	$0.158^{+0.024}_{-0.028}$	$0.158^{+0.019}_{-0.021}$	$0.157^{+0.021}_{-0.023}$	0.150 ± 0.019	$0.147^{+0.015}_{-0.017}$
$\Omega_{0,fld}$	$0.769^{+0.055}_{-0.051}$	$0.615^{+0.047}_{-0.043}$	$0.615^{+0.050}_{-0.054}$	$0.629^{+0.041}_{-0.045}$	$0.650^{+0.035}_{-0.032}$
$w_{0,fld}$	$-1.81^{+0.22}_{-0.23}$	$-1.171^{+0.109}_{-0.085}$	$-1.168^{+0.109}_{-0.085}$	$-1.133^{+0.089}_{-0.070}$	$-1.158^{+0.064}_{-0.060}$
δ_{DMDE}	< 0.77	$0.41^{+0.21}_{-0.31}$	Unconstrained	< 0.71	$0.28^{+0.13}_{-0.22}$
M_B	$\cdots$	$\cdots$	$-19.404^{+0.022}_{-0.024}$	-19.405 ± 0.018	$-19.375^{+0.017}_{-0.016}$
H_0	> 74.12	$68.58^{+1.30}_{-1.41}$	$68.40^{+0.99}_{-1.07}$	$68.32^{+0.83}_{-0.78}$	$69.66^{+0.79}_{-0.73}$
σ_8	$0.75^{+0.11}_{-0.12}$	$0.657^{+0.066}_{-0.075}$	$0.661^{+0.071}_{-0.083}$	$0.682^{+0.067}_{-0.074}$	$0.702^{+0.059}_{-0.063}$
Minimum χ^2	2773.16	2792.32	3805.90	3819.16	3834.68
Δ_{AIC}	-3.54	3.50	1.48	2.40	-1.90

Figure 5 illustrates the two-dimensional allowed contours and the one-dimensional posterior probabilities obtained within model C. Notice that here the situation is just the opposite one of model B: the value of $\Omega_{0,fld}$ is much smaller than in standard scenarios, due to the larger value required for the present matter energy density $\Omega_{0,m}$ when the dark matter–dark energy coupling $\delta_{DMDE} > 0$ and $w_{0,fld} < -1$. This larger value of the present matter energy density also implies a lower value for the clustering parameter σ_8, in contrast to what was required within models A and B, alleviating the σ_8 tension. These two facts (i.e., best-fit model to any of the data combinations plus the alleviation of the σ_8 clustering parameter tension) make model C a very attractive cosmological scenario which can provide a solution for the long-standing H_0 tension. Nevertheless, we must remember here that model C has two degrees of freedom more than the standard ΛCDM paradigm.

V. FINAL REMARKS

In this study we have tried to reassess the ability of interacting dark matter–dark energy cosmologies in alleviating the long-standing and highly significant Hubble constant tension. Despite the fact that in the past these models have been shown to provide an excellent solution to the discrepancy between local measurements and high-redshift (cosmic microwave background) estimates of H_0, there have been recent works in the literature questioning their effectiveness, related to a misinterpretation of SH0ES data, which indeed does not directly extract the value of H_0. We have therefore computed the ability of interacting cosmologies of reducing the Hubble tension by means of a prior on type Ia supernova absolute magnitude, which is more robust and avoids double-counting issues when it is combined with type Ia SN luminosity distance observations. We combine this prior with CMB, type Ia SN and BAO measurements, showing that despite the value of the Hubble parameter being larger, in general, there is no significant preference for interacting dark energy, and in some cosmologies the well-known σ_8 tension worsens. There is however one among the interacting cosmologies considered here, with a phantom nature, which provides a better fit than the canonical ΛCDM framework for all the considered data combinations, is preferred over the canonical ΛCDM picture from CMB data alone and alleviates the σ_8 problem. Nevertheless, this model has two extra degrees of freedom, both describing exotic dark energy physics. Future galaxy surveys will be able to further test these nonstandard dark energy cosmologies by accurately extracting the value of the dark energy equation of state and its possible redshift evolution.
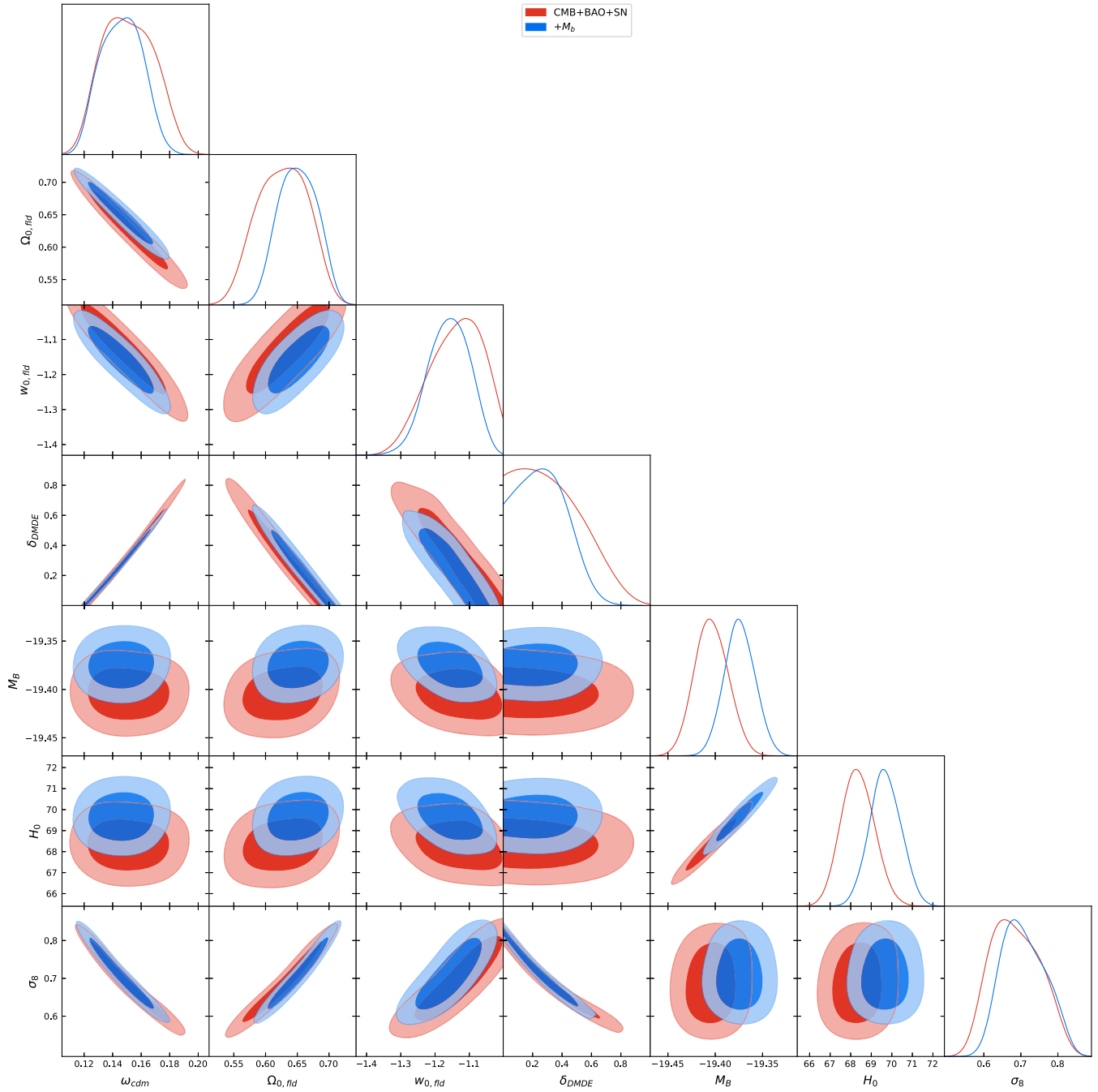
FIG. 5.   68% C.L. and 95% C.L. allowed contours and one-dimensional posterior probabilities on a selection of cosmological parameters within model C, considering two data combinations: CMB + SN + BAO (red) and CMB + SN + BAO + M_B (blue).

[1] W. L. Freedman, Nat. Astron. **1**, 0121 (2017).

[2] E. Di Valentino *et al.*, Astropart. Phys. **131**, 102605 (2021).

[3] E. Di Valentino *et al.*, Astropart. Phys. **131**, 102604 (2021).

[4] E. Di Valentino *et al.*, Astropart. Phys. **131**, 102607 (2021).

[5] W. L. Freedman, Astrophys. J. **919**, 16 (2021).

[6] E. Di Valentino, O. Mena, S. Pan, L. Visinelli, W. Yang, A. Melchiorri, D. F. Mota, A. G. Riess, and J. Silk, Classical Quantum Gravity **38,** 153001 (2021).

[7] N. Schöneberg, G. Franco Abellán, A. Pérez Sánchez, S. J. Witte, V. Poulin, and J. Lesgourgues, arXiv:2107.10291.

[8] R. C. Nunes and S. Vagnozzi, Mon. Not. R. Astron. Soc. **505,** 5427 (2021).

[9] L. Perivolaropoulos and F. Skara, arXiv:2105.05208.

[10] P. Shah, P. Lemos, and O. Lahav, Astron. Astrophys. Rev. **29,** 9 (2021).

[11] E. Abdalla *et al.,* J. High Energy Astrophys. **34,** 49 (2022).

[12] L. Verde, T. Treu, and A. G. Riess, Nat. Astron. **3,** 891 (2019).

[13] A. G. Riess, Nat. Rev. Phys. **2,** 10 (2019).

[14] E. Di Valentino, Mon. Not. R. Astron. Soc. **502,** 2065 (2020).

[15] N. Aghanim *et al.* (Planck Collaboration), Astron. Astrophys. **641,** A6 (2020).

[16] A. G. Riess *et al.,* arXiv:2112.04510.

[17] D. W. Pesce *et al.,* Astrophys. J. Lett. **891,** L1 (2020).

[18] J. P. Blakeslee, J. B. Jensen, C.-P. Ma, P. A. Milne, and J. E. Greene, Astrophys. J. **911,** 65 (2021).

[19] T. de Jaeger, L. Galbany, A. G. Riess, B. E. Stahl, B. J. Shappee, A. V. Filippenko, and W. Zheng, Mon. Not. R. Astron. Soc. **514,** 4620 (2022).

[20] S. Birrer *et al.,* Astron. Astrophys. **643,** A165 (2020).

[21] B. P. Abbott *et al.* (The LIGO Scientific and The Virgo, The Las Cumbres Observatory, The 1M2H, The DLT40, The MASTER, The VINROUGE, The Dark Energy Camera GW-EM and the DES Collaborations), Nature (London) **551,** 85 (2017).

[22] S. Alam, M. Aubert, S. Avila, C. Balland, J. E. Bautista, M. A. Bershady, D. Bizyaev, M. R. Blanton, A. S. Bolton, J. Bovy *et al.,* Phys. Rev. D **103,** 083533 (2021).

[23] O. H. Philcox, M. M. Ivanov, M. Simonović, and M. Zaldarriaga, J. Cosmol. Astropart. Phys. 05 (2020) 032.

[24] O. H. Philcox and M. M. Ivanov, Phys. Rev. D **105,** 043517 (2022).

[25] F. Okamatsu, T. Sekiguchi, and T. Takahashi, Phys. Rev. D **104,** 023523 (2021).

[26] R. C. Nunes and A. Bernui, Eur. Phys. J. C **80,** 1025 (2020).

[27] S. Vagnozzi, F. Pacucci, and A. Loeb, Implications for the Hubble tension from the ages of the oldest astrophysical objects (to be published), arXiv:2105.10421.

[28] T. M. C. Abbott *et al.,* Mon. Not. R. Astron. Soc. **480,** 3879 (2018).

[29] T. M. C. Abbott *et al.,* Phys. Rev. D **105,** 043512 (2022).

[30] A. G. Riess, S. Casertano, W. Yuan, J. B. Bowers, L. Macri, J. C. Zinn, and D. Scolnic, Astrophys. J. Lett. **908,** L6 (2021).

[31] D. M. Scolnic *et al.,* Astrophys. J. **859,** 101 (2018).

[32] D. Camarena and V. Marra, Mon. Not. R. Astron. Soc. **495,** 2630 (2020).

[33] G. Efstathiou, Mon. Not. R. Astron. Soc. **505,** 3866 (2021).

[34] D. Camarena and V. Marra, Mon. Not. R. Astron. Soc. **504,** 5164 (2021).

[35] G. Alestas, L. Kazantzidis, and L. Perivolaropoulos, Phys. Rev. D **103,** 083517 (2021).

[36] V. Marra and L. Perivolaropoulos, Phys. Rev. D **104,** L021303 (2021).

[37] G. Alestas, D. Camarena, E. Di Valentino, L. Kazantzidis, V. Marra, S. Nesseris, and L. Perivolaropoulos, Phys. Rev. D **105,** 063538 (2022).

[38] L. Amendola, Phys. Rev. D **62,** 043511 (2000).

[39] S. Kumar and R. C. Nunes, Phys. Rev. D **94,** 123511 (2016).

[40] R. Murgia, S. Gariazzo, and N. Fornengo, J. Cosmol. Astropart. Phys. 04 (2016) 014.

[41] S. Kumar and R. C. Nunes, Phys. Rev. D **96,** 103511 (2017).

[42] E. Di Valentino, A. Melchiorri, and O. Mena, Phys. Rev. D **96,** 043503 (2017).

[43] W. Yang, S. Pan, L. Xu, and D. F. Mota, Mon. Not. R. Astron. Soc. **482,** 1858 (2019).

[44] W. Yang, S. Pan, E. Di Valentino, R. C. Nunes, S. Vagnozzi, and D. F. Mota, J. Cosmol. Astropart. Phys. 09 (2018) 019.

[45] W. Yang, O. Mena, S. Pan, and E. Di Valentino, Phys. Rev. D **100,** 083509 (2019).

[46] S. Kumar, R. C. Nunes, and S. K. Yadav, Eur. Phys. J. C **79,** 576 (2019).

[47] S. Pan, W. Yang, E. Di Valentino, E. N. Saridakis, and S. Chakraborty, Phys. Rev. D **100,** 103520 (2019).

[48] S. Pan, W. Yang, C. Singha, and E. N. Saridakis, Phys. Rev. D **100,** 083539 (2019).

[49] E. Di Valentino, A. Melchiorri, O. Mena, and S. Vagnozzi, Phys. Dark Universe **30,** 100666 (2020).

[50] E. Di Valentino, A. Melchiorri, O. Mena, and S. Vagnozzi, Phys. Rev. D **101,** 063502 (2020).

[51] E. Di Valentino and O. Mena, Mon. Not. R. Astron. Soc. **500,** L22 (2020).

[52] E. Di Valentino, A. Melchiorri, O. Mena, S. Pan, and W. Yang, Mon. Not. R. Astron. Soc. **502,** L23 (2021).

[53] A. Gómez-Valent, V. Pettorino, and L. Amendola, Phys. Rev. D **101,** 123513 (2020).

[54] W. Yang, S. Pan, R. C. Nunes, and D. F. Mota, J. Cosmol. Astropart. Phys. 04 (2020) 008.

[55] M. Lucca and D. C. Hooper, Phys. Rev. D **102,** 123502 (2020).

[56] M. Martinelli, N. B. Hogg, S. Peirone, M. Bruni, and D. Wands, Mon. Not. R. Astron. Soc. **488,** 3423 (2019).

[57] W. Yang, E. Di Valentino, O. Mena, S. Pan, and R. C. Nunes, Phys. Rev. D **101,** 083509 (2020).

[58] Y.-H. Yao and X.-H. Meng, Phys. Dark Universe **30,** 100729 (2020).

[59] S. Pan, W. Yang, and A. Paliathanasis, Mon. Not. R. Astron. Soc. **493,** 3114 (2020).

[60] Y. Yao and X.-H. Meng, Phys. Dark Universe **33,** 100852 (2021).

[61] H. Amirhashchi and A. K. Yadav, Phys. Dark Universe **36,** 101043 (2022).

[62] W. Yang, S. Pan, E. Di Valentino, O. Mena, and A. Melchiorri, J. Cosmol. Astropart. Phys. 10 (2021) 008.

[63] L.-Y. Gao, Z.-W. Zhao, S.-S. Xue, and X. Zhang, J. Cosmol. Astropart. Phys. 07 (2021) 005.

[64] M. Lucca, Phys. Dark Universe **34,** 100899 (2021).

[65] S. Kumar, Phys. Dark Universe **33,** 100862 (2021).

[66] W. Yang, S. Pan, L. Aresté Saló, and J. de Haro, Phys. Rev. D **103**, 083520 (2021).

[67] M. Lucca, Phys. Rev. D **104**, 083510 (2021).

[68] A. Halder and M. Pandey, Mon. Not. R. Astron. Soc. **508**, 3446 (2021).

[69] M. G. Dainotti, B. De Simone, T. Schiavone, G. Montani, E. Rinaldi, and G. Lambiase, Astrophys. J. **912**, 150 (2021).

[70] R. C. Nunes and E. Di Valentino, Phys. Rev. D **104**, 063529 (2021).

[71] J. Valiviita, E. Majerotto, and R. Maartens, J. Cosmol. Astropart. Phys. 07 (2008) 020.

[72] M. B. Gavela, D. Hernandez, L. Lopez Honorez, O. Mena, and S. Rigolin, J. Cosmol. Astropart. Phys. 07 (2009) 034; 05 (2010) E01.

[73] M. B. Gavela, L. Lopez Honorez, O. Mena, and S. Rigolin, J. Cosmol. Astropart. Phys. 11 (2010) 044.

[74] R. C. Nunes, S. Vagnozzi, S. Kumar, E. D. Valentino, and O. Mena, Phys. Rev. D **105**, 123506 (2022).

[75] J.-H. He, B. Wang, and E. Abdalla, Phys. Lett. B **671**, 139 (2009).

[76] R. C. Nunes, S. Pan, and E. N. Saridakis, Phys. Rev. D **94**, 023508 (2016).

[77] S. Kumar and R. C. Nunes, Phys. Rev. D **94**, 123511 (2016).

[78] B. Wang, E. Abdalla, F. Atrio-Barandela, and D. Pavón, Rep. Prog. Phys. **79**, 096901 (2016).

[79] S. Pan, J. de Haro, W. Yang, and J. Amorós, Phys. Rev. D **101**, 123506 (2020).

[80] W. Yang, O. Mena, S. Pan, and E. D. Valentino, Phys. Rev. D **100**, 083509 (2019).

[81] S. Pan, W. Yang, and A. Paliathanasis, Mon. Not. R. Astron. Soc. **493**, 3114 (2020).

[82] R. Kase and S. Tsujikawa, Phys. Rev. D **101**, 063511 (2020).

[83] R. Kase and S. Tsujikawa, J. Cosmol. Astropart. Phys. 11 (2020) 032.

[84] S. Pan, G. S. Sharov, and W. Yang, Phys. Rev. D **101**, 103533 (2020).

[85] N. Aghanim et al. (Planck Collaboration), Astron. Astrophys. **641**, A6 (2020).

[86] N. Aghanim et al. (Planck Collaboration), Astron. Astrophys. **641**, A5 (2020).

[87] N. Aghanim et al. (Planck Collaboration), Astron. Astrophys. **641**, A8 (2020).

[88] F. Beutler, C. Blake, M. Colless, D. H. Jones, L. Staveley-Smith, L. Campbell, Q. Parker, W. Saunders, and F. Watson, Mon. Not. R. Astron. Soc. **416**, 3017 (2011).

[89] A. J. Ross, L. Samushia, C. Howlett, W. J. Percival, A. Burden, and M. Manera, Mon. Not. R. Astron. Soc. **449**, 835 (2015).

[90] S. Alam et al. (BOSS Collaboration), Mon. Not. R. Astron. Soc. **470**, 2617 (2017).

[91] V. de Sainte Agathe et al., Astron. Astrophys. **629**, A85 (2019).

[92] M. Blomqvist et al., Astron. Astrophys. **629**, A86 (2019).

[93] D. Blas, J. Lesgourgues, and T. Tram, J. Cosmol. Astropart. Phys. 07 (2011) 034.

[94] J. Lesgourgues, arXiv:1104.2932.

[95] T. Brinckmann and J. Lesgourgues, Phys. Dark Universe **24**, 100260 (2019).

[96] N. Aghanim et al. (Planck Collaboration), Astron. Astrophys. **641**, A5 (2020).

[97] D. Camarena and V. Marra, CalPriorSNIa, Publicly available at https://github.com/valerio-marra/CalPriorSNIa.

[98] D. Camarena and V. Marra, Phys. Rev. Research **2**, 013028 (2020).

[99] A. R. Liddle, Mon. Not. R. Astron. Soc. **377**, L74 (2007).

[100] R. Trotta, Contemp. Phys. **49**, 71 (2008).

[101] T. M. C. Abbott et al. (DES Collaboration), Phys. Rev. D **105**, 023520 (2022).

[102] M. Asgari et al. (KiDS Collaboration), Astron. Astrophys. **645**, A104 (2021).

[103] E. Di Valentino, A. Melchiorri, and J. Silk, Phys. Lett. B **761**, 242 (2016).